

# Towards the reconstruction of wide historical sites: A local graph-based representation to resample gigantic acquisitions

Arnaud Bletterer<sup>1</sup>, Frédéric Payan<sup>1</sup>, Marc Antonini<sup>1</sup> and Anis Meftah<sup>2</sup>

<sup>1</sup>Université Côte d'Azur, CNRS, I3S

<sup>2</sup>Cintoo3D

---

## Abstract

Nowadays, LiDAR scanners are able to digitize very wide historical sites, leading to point clouds composed of billions of points. These point clouds are able to describe very small objects or elements disseminated in these sites, but also exhibit numerous defects in terms of sampling quality. Moreover, they sometimes contain too many samples to be processed as they are. In this paper, we propose a local graph-based structure to deal with the set of LiDAR acquisitions of a digitization campaign. Each acquisition is considered as a graph representing the local behavior of the captured surface. Those local graphs are then connected together to obtain a single and global representation of the original scene. This structure is particularly suitable for resampling gigantic points clouds. We show how we can reduce the number of points drastically while preserving the visual quality of large and complex sites, whatever the number of acquisitions.

Categories and Subject Descriptors (according to ACM CCS): I.4.8 [Image Processing and Computer Vision]: Scene Analysis—Range data I.3.5 [Computer Graphics]: Computational Geometry and Object Modeling—Geometric algorithms, languages, and systems

---

## 1. Introduction

Many initiatives are under way to store and share digitally cultural heritage all over the world. Since two decades now, strong attention has been given towards 3D scanning methods. There are many purposes of such an application like digital archiving, physical replication, remote fruition, digital restoration, monitoring of cultural heritage [PGA01]...

There exists a broad range of processes allowing to obtain 3D digital representation of real-life objects such as laser scanning, shape from X (structured light, silhouette, stereo, video, shading, photometry, focus, shadow), or even contact systems [PKA\*07]. The use of one instead of another depends on a broad range of criteria like area of the region to capture, precision of the measures, duration of the acquisition campaign, and so on. Overall, one can decompose the 3D digitization process into two main steps : *acquisition* and *aggregation*.

The first step consists in the capture of the elements composing the region of interest. For this, acquisition systems are moved to different positions, in order to acquire information from different points of view. Such data is then processed into the second step, which assembles the different pieces acquired independently. This step can be quite different between two distinct processes, as the data which has to be merged might not be of the same type. In a context of shape from X, the data acquired are classical 2D images, and 3D points are extracted from such images during this merging

process. In a context of laser scanning, the acquired data are already 3D points, but defined in the local coordinate frame of the scanner. Thus, the aggregation process consists in the registration of all the points in a single world coordinate frame.

In the end, all of those methods provide a point cloud representing samples on the surface of the captured scene. However, such a representation is rarely used as this. For example, for visualization, visual perception can be better if the inherent surface is displayed instead of such a point cloud. Also, when replicating an object, by stereolithography for instance, a polygonal model must be constructed from the point cloud before its creation. Finally, those usages though not being an exhaustive list of the possibilities always require the reconstruction of surfaces from the point clouds generated.

## 2. Related work

The accuracy of LiDAR acquisition systems has considerably increased over the years. Such a technological evolution make it possible to obtain extremely precise acquisitions, up to 1mm accuracy. This means that nowadays such equipments can be used to obtain an overall description of a cultural heritage site, but also to capture very small details, despite the huge area of the region they cover.

Having such a precision while digitizing a whole site results in point clouds which can contain several billions of points. More-

over, those point clouds are the result of the merging of different acquisitions taken at different locations. Thus, they exhibit numerous defects in terms of sampling quality (highly non-uniform distributions, noise, etc.), and may contain too many samples to be processed as they are. These drawbacks limit their usage and their sharing, and make some processings very complex, or even impossible (surface reconstruction for instance).

Resampling the data is one solution to tackle this problem, but this is not straightforward for such particular data. There are mainly two reasons. Firstly, point clouds are often *unstructured*, which makes their management complex, in particular because the knowledge of the underlying surface is a valuable information that is missing. Secondly, massive point clouds may not fit in memory, and discard many in-core algorithms from being used on standard desktop machines.

The most common approach is to construct space partitioning trees to structure and then to manage the point clouds. Several methods already exist [PK05, SZW09, RH10, RGM\*12, LZZ13, HWB\*13, EBN13]. Those methods have the advantage to process unstructured point clouds without any *a priori* on their origin. But, given the specificities of our data - wide sites with various small details - those representations may be inappropriate, because the domain of definition of the captured samples is a surface, and not the 3D space. For example, without additional processing, using normals for instance, these methods are unable to take into account the behavior of the surface throughout the points.

An important point to note though, is that such methods aim at providing solutions to interactively visualize or compress dense sets of points, using different strategies to extract relevant information from the constructed trees quickly. As a result, they never explicitly extract a resampled version of a point cloud for further processings.

Recently, [CTF\*18] proposed to use a graph to describe a point cloud. This structure has the advantage to take into account the topology of the captured surface, which is convenient to apply classical signal processings, such as resampling. Unfortunately, this global structure is not really scalable, and finally is inappropriate to deal with our gigantic acquisitions.

### 3. General overview

In this paper, we propose an alternative solution to the work of [CTF\*18]. The idea is to construct a local graph for each LiDAR acquisition, before merging all of them as a single point cloud. Our main motivation relies on the fact that each acquisition provides a depth map that is a structured representation of a part of the acquired surface. We consider these graphs as *local*, because each of them describes only a subset of the whole point cloud. Then, to process the point clouds in a globally coherent manner, but also to avoid redundant computations in the overlapping regions, we also propose a solution to "connect" our local graphs. This enables, when dealing with a specific graph, to transmit/fetch various information to/from the other graphs representing the same regions. To show the interest of such a structure in practice, we consider it to resample gigantic point clouds merging multiple LiDAR acquisitions, *via* a Poisson-disk sampling strategy.

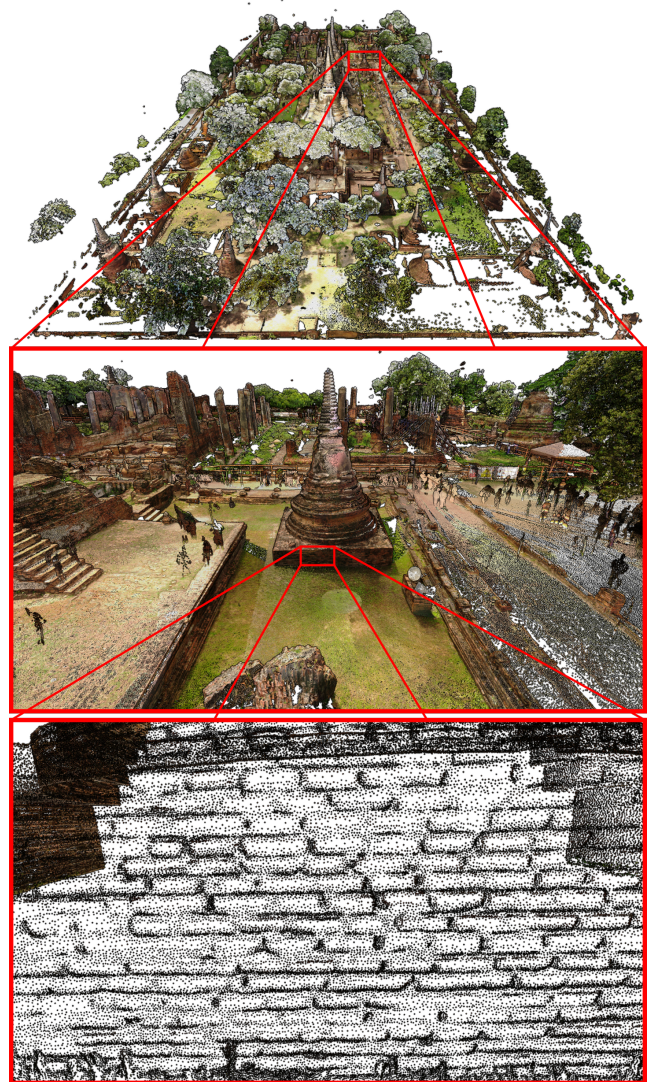


**Figure 1:** The site Wat Phra Si Sanphet, Ayutthaya (Thailand), resampled with our graph-based approach. The original data contain more than 5 billion points, merging 156 different acquisitions. We are able to represent it with only 2.8% of the original number of points while preserving fine-scale details (such as bricks in a wall over a  $40.000\text{m}^2$  area).

Our local graph-based resampling has many advantages. First, the memory required for any local processing is bounded by the number of graphs involved, which enables to deal with gigantic points clouds. Second, it provides some guarantees with respect to the covering of the captured surface. Third, by modifying the metric associated to each graph, fine details can be preserved even in large-scale scenes. In this paper, we show how our method is particularly relevant for resampling acquisitions of cultural heritage sites (see Figure 1) that generally merge numerous scans, to reach more than a billion of points. We also show how it enables the use of surface

reconstruction algorithms to recover the underlying surface of those gigantic acquisitions, and the level of detail that can be recovered.

The rest of the paper is organized as follows. Section 4 provides a background on the notions of depth maps and Poisson disk sampling. In Section 5, we introduce our local graph-based representation as a way to structure a set of acquisitions. In Section 6, we present a surface-aware resampling strategy using the local graphs proposed. In Section 7, several experimentations are shown on large and complex cultural heritage sites, both in terms of timings and visual quality as well as reconstructions obtained from our samplings.

## 4. Background

For a good understanding of our motivations, we explain in this section the characteristics of the native structure of the captured data, namely depth maps, as well as a basic introduction to the sampling process considered in this work, the Poisson-disk sampling.

### 4.1. Depth maps

A depth map  $D$  (also called range image) is a 2-dimensional image whose intensities represent the distance between the points acquired in the scene, and the position of the acquisition system. A depth map is composed of *valid pixels*, i.e., acquired points, and *non-valid pixels*, representing directions with no depth information and identified by having a null intensity. Depth maps can be provided by different kinds of acquisition devices (capture of real-life scenes), but also created synthetically from any 3D digital model (similarly to the work of [PTSZ11]).

Combined with its parameterization function (a mapping from 3D to 2D), a depth map is *geometrically equivalent* to a point cloud. A depth map also gives an information about the *surface topology*, which has to be recovered when processing the resulting point cloud only. Finally, depth maps naturally provide a suitable domain to deal with the captured surface, e.g., for neighborhood requests, subsampling, filtering, etc.

More formally, a depth map  $DM$  is a parameterization of a point cloud  $PC$  acquired from a specific position and orientation.  $DM$  is obtained by using a parameterization function  $c$ , such that  $DM = c(PC)$ . This function is invertible, which means that  $PC = c^{-1}(DM)$ .  $c$  is called the *projection* and  $c^{-1}$  the *embedding*.

In our context, the depth maps come from terrestrial LiDARs. In this case, the position  $p = (m, n) \in \mathbb{N}^2$  of a pixel represent respectively the azimuthal angle  $\theta$  and the polar angle  $\varphi$ , and its intensity  $\mathcal{I}(p)$  represents the radial distance  $r$  (all representing a spherical coordinates system centered on the position of a LiDAR during the acquisition). The function  $c$  can be expressed as a change of coordinates. Let  $p_w = (x, y, z)$  be a 3D point in the cartesian world coordinate system. Its coordinates in a cartesian coordinate system centered on the scanner during the  $i$ th acquisition are obtained by using a rotation matrix  $R_{s_i}$  and a translation vector  $T_{s_i}$ :

$$\begin{pmatrix} x_{s_i} \\ y_{s_i} \\ z_{s_i} \end{pmatrix} = p_{s_i} = R_{s_i}(p_w - T_{s_i}).$$

Then, the conversion to spherical coordinates can be done :

$$\begin{aligned} r_{s_i} &= \sqrt{x_{s_i}^2 + y_{s_i}^2 + z_{s_i}^2}, \\ \theta_{s_i} &= \tan^{-1}\left(\frac{y_{s_i}}{x_{s_i}}\right), \\ \varphi_{s_i} &= \cos^{-1}\left(\frac{z_{s_i}}{r_{s_i}}\right). \end{aligned}$$

Finally, the coordinates in the depth map  $p_i = (m_{s_i}, n_{s_i})$  can be obtained by quantizing  $\theta_{s_i}$  and  $\varphi_{s_i}$  with respect to the resolution of the depth map  $DM$ .

### 4.2. Poisson-disk sampling

Due to its *blue noise* characteristics, *Poisson-disk sampling* is a common sampling strategy in Computer Graphics (see [Coo86] and [Uli88] for more details). A Poisson-disk sampling generates a random distribution of samples on a plane  $H$ , while imposing a *minimum distance* between them. This minimum distance is controlled by using disks of radius  $r$ , centered on each sample, such that no disk overlaps any other one. Consequently, the disks ensure a *lower bound* on the distances between samples :

$$\forall s_i, s_j \in S, i \neq j, \|s_i - s_j\| > 2r, \quad (1)$$

where  $S \subset H$  represents the set of samples.

A Poisson-disk sampling is said to be *maximal* if no sample can be added anymore. In this case, the *maximum distance* between any point in the plane and its closest sample is directly related to the radius  $r$  is strictly lower than  $2r$ , as for any point located at a distance  $2r$  of a sample a new sample with a disk of radius  $r$  could be added without overlapping any other disk. Thus, a maximal Poisson-disk sampling also ensures an *upper bound* of the distance between any point  $x \in H$  and the closest sample:

$$\forall x \in H, \exists s \in S, \|x - s\| < 2r. \quad (2)$$

In our context, this gives guarantees about the covering of the domain.

Over the years, generalizations have been done, to sample  $n$ -dimensional domains quite efficiently [Bri07]. Research has also been oriented towards non-uniform domains, e.g., on surfaces [BWW10, CCS12, PPA15], and/or algorithms efficiency. For example, [PPA15] has shown that a low complexity sampling could be achieved by considering a discrete approach of the popular *dart throwing* technique [Coo86] to sample surfaces.

## 5. A set of local graphs to describe the captured surface

The work of [CTF\*18] gives theoretical ideas that demonstrate the interest of constructing graphs over point clouds, for applying signal processing tools afterward. By associating a topology to a point cloud, graphs are particularly suitable to process its underlying surface, instead of its ambient space. As pointed out by the authors, a graph is a generalization of a polygonal mesh, but whose construction is easier, since connectivity restrictions existing in polygonal meshes are relaxed.

Nevertheless, the construction of a single graph over the whole point cloud is far too expensive to be done on massive data for now.

Instead, we propose to construct a set of *local graphs*, each graph describing a part of the underlying surface of a point cloud.

### 5.1. Construction

At each acquisition, a terrestrial LiDAR scanner provides a depth map. As a depth map can be seen as a structured representation of the captured scene, we consider its connectivity to construct a local graph representing the part of the surface captured by this acquisition.

However, simply transposing a depth map as a graph may be inefficient. First, acquisitions are generally *noisy*, because of the external conditions during the acquisition (ambient light, surface shininess, dust and moisture in the atmosphere, ...). Secondly, for a given depth map, neighboring pixels are not necessarily associated to points geodesically close on the underlying surface, because of *occlusions* but also obtuse scanning angles that can appear, depending on the position of the LiDAR.

**Dealing with noisy acquisitions** In order to lower the impact of the noise during the computations, without degrading the accuracy of an acquisition, we first apply a bilateral filtering [AW95, SB97, TM98] on the depth map. Following notations of [PKTD07], we recall that a bilateral filter is a non linear filter that smoothes a signal while preserving strong edges:

$$\hat{D}(p) = \frac{1}{W_p} \sum_{q \in \Omega_p} \mathcal{I}_q G_{\sigma_s}(\|p - q\|) G_{\sigma_r}(|\mathcal{I}(p) - \mathcal{I}(q)|), \quad (3)$$

where  $\hat{D}$  is the denoised depth map,  $G_{\sigma_s}$  is a gaussian function taking into account the spatial closeness, and  $G_{\sigma_r}$  is a gaussian function taking into account the intensity difference.  $W_p$  corresponds to the normalization factor :

$$W_p = \sum_{q \in \Omega_p} G_{\sigma_s}(\|p - q\|) G_{\sigma_r}(|\mathcal{I}(p) - \mathcal{I}(q)|).$$

This filtering reduces the noise present in a depth map - and in the point cloud, by invariance of the association - without merging different regions with strong depth variations (see Figure 2). In the rest of the section, we will refer to  $D$  as being the filtered depth map  $\hat{D}$ .

**Dealing with the occlusions** As typical scenes are composed of various elements, many different objects may appear close once projected into a depth map, even if they are not next to each other on the surface. Figure 3 illustrates the problem in a nutshell: because of the occlusions, some neighboring pixels do not correspond to neighboring points on the corresponding surface.

Most of the time, when two neighboring pixels in a given depth map belong to two distinct elements in the scene, their depths strongly vary. Therefore high depth variations are detected to identify vertices which should not be linked together in the graph. Technically, we compute morphological gradients  $g(D)$  [RSB93] on the depth map  $D$  :

$$g(D) = D \oplus b - D \ominus b,$$

where  $b$  is a structuring element, and  $\oplus$  and  $\ominus$  are the dilation and erosion operations, respectively. Then, we tag as non-valid the pixels with high gradients, by considering an adaptive thresholding on

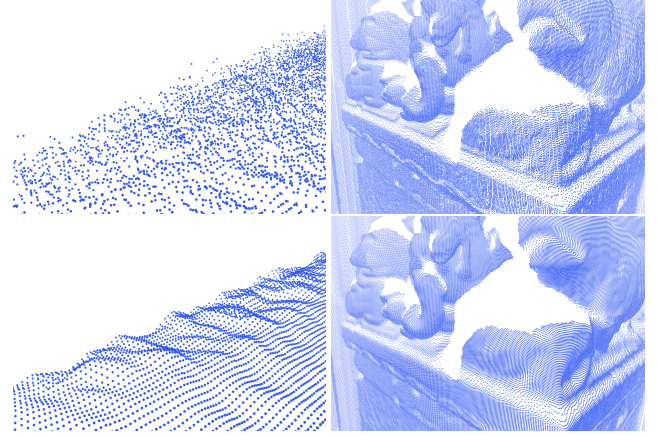


**Figure 2:** Impact of the bilateral filtering on a given depth map, on the quality of the point cloud (top: before filtering ; bottom : after filtering). Close-up view of St Trophime.

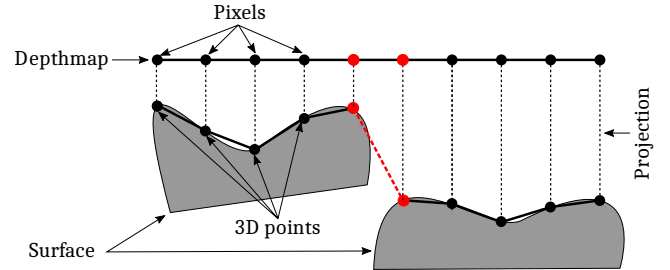


**Figure 3:** Typical case of connectivity in the parameterization domain provided by the depth map that is not faithful to the topology of the acquired surface: two objects in the acquired scene are projected onto neighboring pixels, but the red edge must not exist in the graph.

$g(D)$ , to take into account the intensity variation with respect to the distance between a point and the acquisition system. Finally, an *undirected graph*  $G = (V, E)$  is constructed, where the vertices  $V$  correspond to the valid pixels, and the edges  $E$  connect neighboring valid pixels.

### 5.2. Connections between the local graphs

In the context of surface parameterization, when an atlas of charts is constructed, some parts of a manifold can be covered by different charts. In that case, some parts of the parameterization domain of a given chart are mapped to the parameterization domains of the other charts, and vice-versa [GZ06]. This is done with a *transition functions*  $\tau_{ij}$  that transforms points of the parameterization domain  $G_i$  to the parameterization domain  $G_j$  according to the parameterization functions  $c$ :

$$\tau_{ij} = c_j \circ c_i^{-1}.$$

In our context, we consider the acquisition process as the creation of an atlas of charts, where:

- the manifold is the acquired surface,
- a chart corresponds to an acquisition,
- the parameterization domain associated to a chart corresponds to the depth map generated by this acquisition.

Those transition functions could be used to construct a global seamless parameterization, as in [PTSZ11]. But this approach, although being an elegant and implicit solution, is computationally expensive, and thus inappropriate for gigantic acquisitions.

As an alternative solution, we propose to link the vertices of the different graphs that correspond to nearby points on the surface. Hence, each vertex  $v \in V_i$  of a given graph  $G_i(V_i, E_i) \in G$  is associated with  $C_v$ , its set of  $m$  corresponding vertices in the other graphs, using the transition functions between each pair of graphs (when such vertices exist):  $C_v = \{v_0, v_1, v_2, \dots, v_{m-1}\}$ .

From there, a unique graph similar to the one constructed by [CTF\*18], could be obtained by merging corresponding vertices, and then, could be used to apply various signal processing algorithms [SNF\*13]. Unfortunately, in our context of gigantic data, this global graph suffers from its space complexity ( $\mathcal{O}(|V| + |E|)$ ), that makes its management impractical.

Indeed, a cultural heritage site contains multiple points of interest, such as statues at different locations of the site. Thus, a single acquisition is not enough to describe precisely all the different elements belonging to such a scene. As a consequence, a digitization campaign generally consists of several acquisitions done at different positions, which can quickly rise to dozens or even more than a hundred for large-scale scenes.

Therefore, instead of merging the corresponding vertices to consider the links between graphs as implicit, we choose to keep the graphs distinct, and to store the corresponding vertices  $C_v$  associated to each vertex explicitly. Hence, when computing a local processing, only the vertices and the associated edges concerned by this processing are loaded in memory.

### 5.3. Managing the overlapping regions

In overlapping regions, the number of vertices belonging to each graph depends on the position and the resolution of the acquisition device. The density of the graph can have a strong influence on the accuracy of the computations. For example, when estimating distances on the graphs, a denser graph would lead to a more precise estimation of distances. To simplify computations, while getting the most accurate results, we propose to identify the graph with the highest density in each overlapping region. For a specific region, all the operations will be performed from this graph. Then, to ensure coherency between different graphs, once calculations have been done for the vertices of this region, results are transmitted to all their corresponding vertices in the other graphs.

**Identification of the highest density graphs** To identify in which local graph a given calculation has to be done, and from which graph a result can be fetched from another graph, we must determine the sampling density around each vertex, according to its acquisition. For a given vertex  $v_i$ , this can be done by computing its average squared distance to all the vertices  $v_j \in \mathcal{N}_k(v_i)$ ,  $\mathcal{N}_k(v_i)$  being the  $k$ -hop neighborhood of  $v_i$ . The  $k$ -hop neighborhood of  $v_i$

contains the vertices connected to  $v_i$  by at most  $k$  "edge hops". The density  $w(v_i)$  is estimated as being the inverse of this distance :

$$\frac{1}{w(v_i)} = \frac{1}{|\mathcal{N}_k(v_i)|} \sum_{v_j \in \mathcal{N}_k(v_i)} \|v_j - v_i\|^2.$$

Then, for each vertex  $v_i \in V_i$  of each graph  $G_i$ , we compare its density  $w(v_i)$  with the density  $w(v'_i)$  of its corresponding vertices  $v'_i \in C_{v_i}$ . At the end of this process, each set of vertices  $V_i$  of each graph  $G_i$  is decomposed into two sets :

- $V_i^+ \subseteq V_i$ , the set of vertices having the highest density with respect to all their corresponding vertices
- $V_i^- = V_i \setminus V_i^+$ , the remainders.

## 6. Resampling gigantic point clouds using local graphs

In this section, we present how our local-graph based structure can be used to resample point clouds. First, we present our implementation of the popular Dart throwing algorithm [Coo86] that enables the maximal Poisson-disk sampling of a single LiDAR acquisition. Then, we show it can be extended to a set of overlapping acquisitions to deal with gigantic points clouds.

### 6.1. Graph based dart throwing for a single LiDAR acquisition

The principle of dart throwing is simple. Considering the minimum distance  $2r$  required between two samples, it consists in i) picking out randomly a *candidate* sample on the domain, ii) constructing a disk of radius  $r$  centered on this sample, and iii) verifying if this disk intersects another disk. If not, this candidate belongs to the distribution. Otherwise, this candidate is discarded. To get a maximal Poisson-disk sampling, this process is repeated until no more sample can be "thrown" on the domain without violating the "no disk intersection" constraint.

Algorithm 1 summarizes the procedure.

**Data:**  $V$  : the list of candidate samples

**Result:**  $S^r$  : the set of final samples

```

while  $V$  is not empty do
     $v = V$ .getRandomElement();
     $D_v = \text{constructPoissonDisk}(v, r)$ ;
    if  $D_v$  intersects an existing disk then
         $V$ .removeElement( $v$ );
    else
         $S^r$ .addElement( $v$ );
        for  $v_i \in D_v$  do
             $V$ .removeElement( $v_i$ );
        end
    end
end

```

**Algorithm 1:** Discrete dart throwing algorithm.

The vertices of the graph are the initial list of candidate samples, and the idea is to test the validity of each candidate by constructing its disk over the graph. At the end, the set of samples  $S^r$  corresponds to the final distribution.

The construction of the disks can be done using Dijkstra’s shortest path algorithm [Dij59]. One attractive feature of our graph-based structure is that it is very simple to model different metrics, by simply modifying the weights associated to the edges  $E$ . For example, if we choose as weights the distances between the points in 3D space, then the shortest path from a vertex to another one in the graph represents the shortest path from a point to another point on the surface.

Figure 4 shows a part of a maximal Poisson-disk sampling of the model *St Trophime*, resulting from our graph-based dart throwing. Observe that the construction of the disks is stopped when the silhouette of an object has been reached, taking into account the topology of the captured surface.

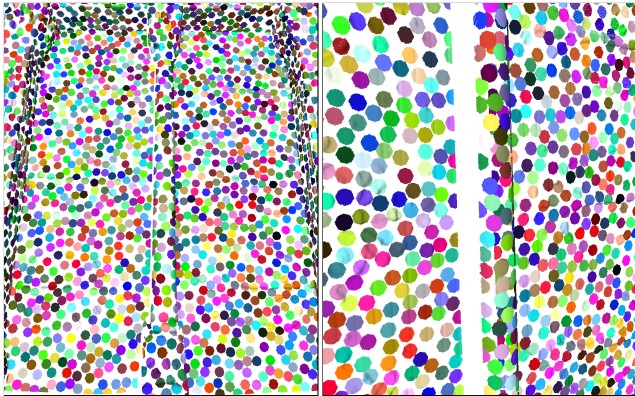


**Figure 4:** Maximal Poisson-disk sampling of one acquisition of *St Trophime*, obtained with our graph-based dart throwing. From left to right : front view and side view.

## 6.2. Resampling a set of 3D acquisitions

Using the local graph approach proposed, the generalization of the Algorithm 1 is fairly elementary. Let us consider the set  $G = \{G_1, G_2, G_3, \dots, G_n\}$  as the set of  $n$  local graphs constructed from  $n$  acquisitions. For each graph  $G_i \in G$ :

- Algorithm 1 is applied on  $G_i$ , with the vertices  $V_i^+$  as candidate samples,
- for each other graph  $G_j \in G, j \neq i$ , vertices  $V_j$  fetch information about the inclusion (or not) to a specific disk of their corresponding vertices in  $V_i$ .

Thanks to the local aspect of the dart throwing, and by relying on the construction and verification of disk intersections, only a part of the total data needs to be considered for each potential sample. As a consequence, only the graphs concerned have to be stored in memory.

## 7. Experimental results

All the experimental results represent real-life scenes of different historical monuments. The acquisitions of *Ananda Oak Kyaung*, *Eim Ya Kyaung*, *Khaymingha*, *St Trophime* and *Wat Phra Si Sanphet* are courtesy of the *CyArk/Google Open Heritage Program*.

The acquisitions of *Grand Palais* are courtesy of *Art Graphique et Patrimoine*.

All the results have been generated on the same computer [Intel Core i7-5960X CPU @ 3.00GHz, NVIDIA Quadro M5000, 32GB of RAM and 1TB SSD drive].

Figure 5 shows the difference of distributions obtained on the model *Grand Palais*, with or without a curvature-aware metric. This curvature-aware metric simply consists in weighting each edge with respect to the curvature between the two vertices linked by this edge. While keeping approximately the same number of points, we can see that the detailed areas are further enhanced. This result highlights the interest of taking into account the curvature during the resampling, which is quite easy thanks to our graph-based approach.

It is interesting to note that one could consider weighting edges with respect to other metrics, and thus sampling more densely some areas instead of others, by considering for instance a weight depending on the position of a point with respect to a region of interest.

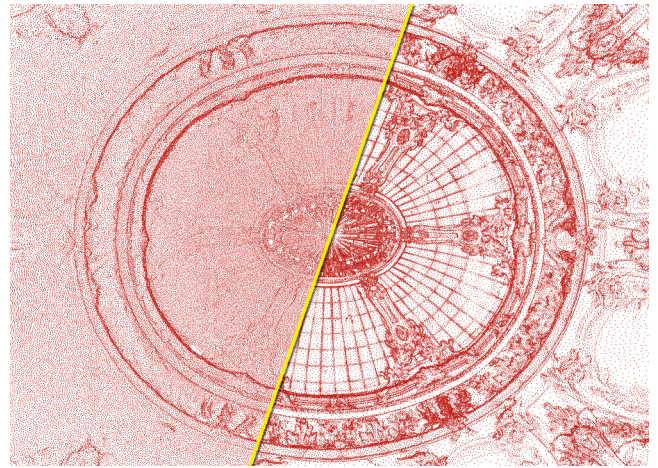


**Figure 5:** Part of the *Grand Palais* (2 billion points, 35 acquisitions) resampled (0.15% of the original number of points) with a uniform distribution (left), or with a curvature-aware distribution (right).

Figure 1 shows the site of *Wat Phra Si Sanphet*, *Ayutthaya*, in *Thailand*, resampled with our graph-based approach. The original data contains more than 5 billion points, divided in 156 acquisitions. Our resampled model contains only 155 millions points. By efficiently distributing the samples according to a curvature-aware approach, we are able to preserve fine-scale details, such as bricks in a wall, despite the expanse of the site.

Another convincing result is shown in Figure 6. It represents a close-up view of a statue of the *Eim Ya Kyaung* temple. Even if this site represents a really big area of 6,000m<sup>2</sup>, modeled by an original point cloud composed of 1.7 billion points, our algorithm is able to process it as a whole. We can see that the resulting samples are well distributed and fit closely areas of high curvature, reducing drastically the number of points (0.6% of the original number of points left) while preserving the shape of small scale elements

present in the site. To have an idea of the error induced during the sampling process, and of its impact on the quality of relevant elements of such a huge site, we also present a color-coded representation of the original point cloud, showing how the error is spread. This error represents the distance from the points of the original point cloud to the closest sample of the final distribution. Thanks to the curvature-aware resampling, we can see that the highest errors (biggest distances between original points and samples of the final distribution) are concentrated in areas of low curvature.

Finally, to attest that the piecewise nature of our approach does not introduce any distortion in terms of sampling quality, Figure 7 gives a close-up view of two overlapping acquisitions. We can see that the graph correspondences enable to get a globally coherent distribution, and that we cannot distinguish any distortion along the borders.

In Table 1, we present the computing times of the proposed algorithm on several gigantic data. The construction of the graphs is the longest step, and represents the bottleneck of our algorithm for the biggest acquisitions. However, for a given set of acquisitions, this construction can be done once and for all, independently of the resampling step. So, the graphs can be saved to be used subsequently, for any further processing, which lowers the impact of those computations. Concerning the resampling step itself, even if the datasets are big and that our approach is working sequentially, the algorithm is able to provide samplings in few hours (more than 500.000 points processed per second for points clouds around one billion points and nearly 400.000 for point clouds around 5 billion points).

### Application to surface reconstruction

To definitively show the interest of our approach in the domain of cultural heritage, Figures 8 and 9 show reconstructions generated with the method of [BL17] from points obtained with our resampling technique. We used [BL17] because it is able to reconstruct efficiently detailed surfaces, and that the vertices of the reconstructed mesh are exactly the input points. The resulting reconstructions are quite remarkable, thanks to the surface-aware behavior of our resampling operation (highlighted by the quality of the final triangulation).

### 8. Discussion

Even if this paper focused on terrestrial LiDARs acquisitions, it is important to note that the proposed local graph structure can be used on a broader range of acquisition systems, such as aerial LiDARs or Kinect-like acquisitions. Though care should be taken when dealing with the noise generated by Kinect-like systems, since this one can be quite different from the one present in terrestrial LiDAR acquisitions.

In undersampled areas, the assumption made about depth disparity to link vertices in the graphs might not hold anymore. In such areas, two problems can occur :

- when the scanner is too far from a region, the distance between two neighboring samples in the depth map might be more important than the size of a hole between two different regions. Thus this would result in a false-negative contour.

- when the laser hits some areas at obtuse angles, the depth between two samples might vary strongly, while still belonging to the same element. This would result in a false-positive contour.

Though, such particularities do not pose problems in practice, because undersampled regions are generally covered by other acquisitions having a higher density.

When creating a graph from an acquisition, different connectivities could be considered. The choice of connectivity gives some compromise between speed (with a low number of edges per vertex) and accuracy (with a higher number of vertices connected together) of the distances computed. In our experiments, we noticed that the 8-connectivity was giving good results, both in terms of speed and accuracy.

For now, we have no guarantee that the resulting distributions will keep all the information present in the original point clouds. This is because the cutting frequency (the radius of the disks) has to be related to the maximal frequency appearing in the spectrum of the point cloud. But to our knowledge, none method is able to compute "frequencies" over massive point clouds like the one presented in this paper. An interesting work would be to study the use of the Laplace-Beltrami operator for such particular data. Though, the provided sampling algorithm gives the guarantee that the error between the point cloud - considered as input of the sampling algorithm - and the final distribution is bounded and will always be proportional the disk radius. Further processes generally precondition the maximum number of points that should be kept from the original point clouds (since it influences the computing time). Thus we think that giving the control on the radius of the disks is something essential, even if it might result in a loss of information (undersampling the original point clouds).

### 9. Conclusion

In this paper we mainly presented two contributions.

Firstly, we introduced a new structure for processing point clouds generated from a set of terrestrial LiDARs. By taking advantage of the structure of depth maps created by LiDARs, local graphs are constructed - describing the local behavior of the surface acquired - and linked together to process the point cloud globally.

Secondly, we presented an efficient resampling method for gigantic point clouds, based on our local graph structure. Our objective was to reduce the number of points without altering the visual quality of large and complex sites. Sampling each graph using a maximal Poisson disk sampling ensures a good local quality of the distribution. Correspondences between those graphs enable an efficient resampling of overlapping regions, ensuring a good quality of the distribution globally.

Experimental results have shown that our algorithm is able to take into account the behavior and the local details of the captured surfaces efficiently. In particular we showed that our method generates good curvature-aware resamplings even on gigantic point clouds, and enables surface reconstructions of high quality.

This work has promising perspectives. We are convinced that using a set of connected graphs taking advantage of the topology of



**Figure 6:** Close-up view of a statue inside the Eim Ya Kyaung temple. Despite the size and complexity of the scene (1.7 billion of points, 58 acquisitions spread over 6,000 m<sup>2</sup>), our resampling preserves very fine details with only 0.6% of the original number of samples. Maximum error: 6.3cm (between the legs of the statue); Mean error: 0.8cm. Left: original data; middle: our curvature-aware resampling; right: color-coded difference between the original point cloud and the resulting distribution (blue: low error; red: big error). It is interesting to note that the adaptive resampling strategy concentrates the highest errors in the areas of low absolute curvature, where few details are present.

Model	In	Acquisitions	Construction (h:m)	Out	Sampling (h:m)
Khaymingha Bagan, Myanmar	1,383M	74	00:59	44.8M	00:39
				21.2M	00:39
				9.2M	00:46
Ananda Oak Kyaung Bagan, Myanmar	1,703M	126	02:14	41.9M	00:56
				21.9M	00:55
				11.6M	01:01
Wat Phra Si Sanphet Ayutthaya, Thailand	5,313M	156	11:56	148.2M	03:49
				76.3M	03:44
				37.9M	03:50

**Table 1:** Performances of our resampling algorithm on real-life acquisitions. **In** represents the number of points of the original point cloud. **Out** the number of points of the resulting distributions. **Construction** represents the time to construct the local graphs structure. **Sampling** represents the time to sample each graph and to transmit information between graphs. All timings include reading/writing time from/to the disks.

the acquisitions is a relevant structure for many other point cloud processings. For instance, we are currently working on a surface reconstruction algorithm based on the proposed structure.

### Acknowledgements

Thanks to the anonymous reviewers for their insightful comments. This work is supported by a grant from *Région Provence Alpes Côte d’Azur* (France).

### References

- [AW95] AURICH V., WEULE J.: Non-linear gaussian filters performing edge preserving diffusion. In *Mustererkennung 1995*. Springer, 1995, pp. 538–545. 4
- [BL17] BOLTCHÉVA D., LEVY B.: Surface reconstruction by computing restricted voronoi cells in parallel. *Computer-Aided Design* 90 (2017), 123–134. 7, 9, 10
- [Bri07] BRIDSON R.: Fast poisson disk sampling in arbitrary dimensions. In *SIGGRAPH sketches* (2007), p. 22. 3
- [BWW10] BOWERS J., WANG R., WEI L.-Y., MALETZ D.: Parallel poisson disk sampling with spectrum analysis on surfaces. *ACM Transactions on Graphics (TOG)* 29, 6 (2010), 166. 3
- [CCS12] CORSINI M., CIGNONI P., SCOPIGNO R.: Efficient and flexible sampling with blue noise properties of triangular meshes. *IEEE Transactions on Visualization and Computer Graphics* 18, 6 (2012), 914–924. 3
- [Coo86] COOK R. L.: Stochastic sampling in computer graphics. *ACM Trans. Graph.* 5, 1 (Jan. 1986), 51–72. URL: <http://doi.acm.org/10.1145/7529.8927>, doi:10.1145/7529.8927. 3, 5
- [CTF\*18] CHEN S., TIAN D., FENG C., VETRO A., KOVAČEVIĆ J.: Fast resampling of three-dimensional point clouds via graphs. *IEEE Transactions on Signal Processing* 66, 3 (2018), 666–681. 2, 3, 5
- [Dij59] DIJKSTRA E. W.: A note on two problems in connexion with graphs. *Numer. Math.* 1, 1 (Dec. 1959), 269–271. URL: <http://dx.doi.org/10.1007/BF01386390>, doi:10.1007/BF01386390. 6
- [EBN13] ELSEBERG J., BORRMANN D., NÜCHTER A.: One billion points in the cloud—an octree for efficient processing of 3d laser scans. *ISPRS Journal of Photogrammetry and Remote Sensing* 76 (2013), 76–88. 2
- [GZ06] GRIMM C., ZORIN D.: *Surface modeling and parameterization with manifolds: Siggraph 2006 course notes*. ACM, 2006. 4
- [HWB\*13] HORNING A., WURM K. M., BENNEWITZ M., STACHNISS C., BURGARD W.: Octomap: An efficient probabilistic 3d mapping framework based on octrees. *Autonomous Robots* 34, 3 (2013), 189–206. 2
- [LZZ13] LOOP C., ZHANG C., ZHANG Z.: Real-time high-resolution sparse voxelization with application to image-based modeling. In *Proceedings of the 5th High-Performance Graphics Conference* (2013), ACM, pp. 73–79. 2

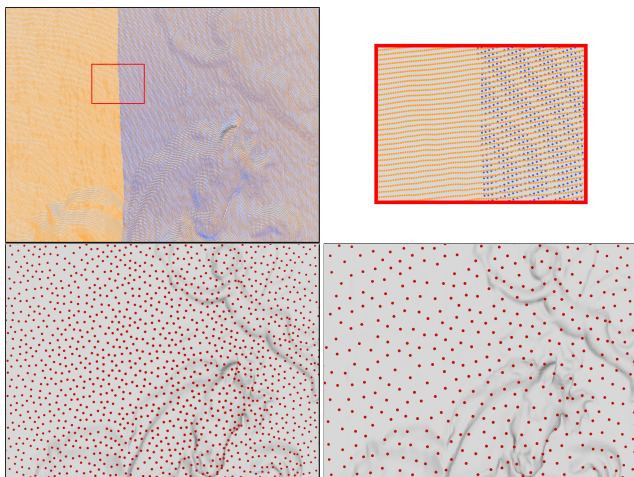


**Figure 7:** Our point clouds do not suffer from any distortion in terms of sampling quality, despite its piecewise nature. Top row: two acquisitions overlapping each other, leading to strong density variations in the original point cloud. Bottom row: two uniform distributions, with different densities, obtained with our graph-based approach. For visualization purposes, low density samplings have been targeted.

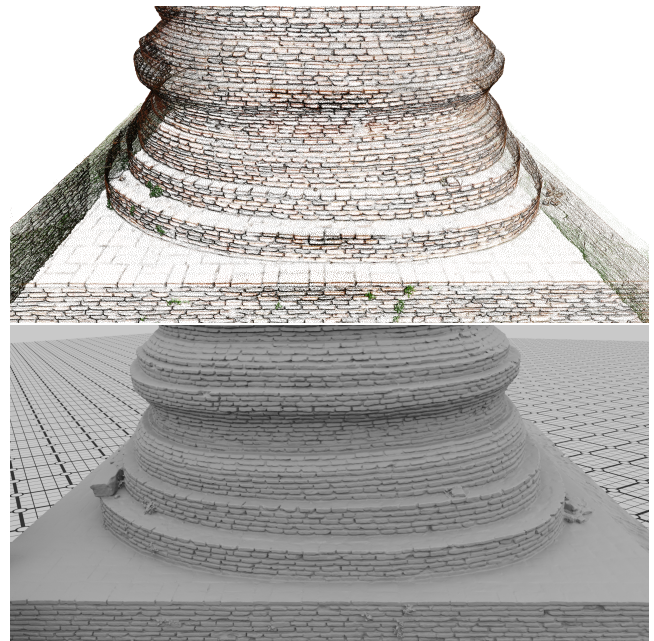


**Figure 8:** Part of a sampling generated from the Wat Phra Si Sanphet site, and reconstruction obtained considering those selected samples as an input of [BL17].

- [PGA01] PIERACCINI M., GUIDI G., ATZENI C.: 3d digitizing of cultural heritage. *Journal of Cultural Heritage* 2, 1 (2001), 63–70. 1
- [PK05] PENG J., KUO C.-C. J.: Geometry-guided progressive lossless 3d mesh coding with octree (ot) decomposition. In *ACM Transactions on Graphics (TOG)* (2005), vol. 24, ACM, pp. 609–616. 2
- [PKA\*07] PAVLIDIS G., KOUTSOUDIS A., ARNAOUTOGLU F., TSIUKAS V., CHAMZAS C.: Methods for 3d digitization of cultural heritage. *Journal of cultural heritage* 8, 1 (2007), 93–98. 1
- [PKTD07] PARIS S., KORNPBST P., TUMBLIN J., DURAND F.: A gentle introduction to bilateral filtering and its applications. In *ACM SIGGRAPH 2007 courses* (2007), ACM, p. 1. 4
- [PPA15] PEYROT J.-L., PAYAN F., ANTONINI M.: Direct blue noise resampling of meshes of arbitrary topology. *The Visual Computer* 31, 10 (October 2015), 1365–1381. doi:10.1007/s00371-014-1019-1. 3
- [PTSZ11] PIETRONI N., TARINI M., SORKINE O., ZORIN D.: Global parametrization of range image sets. In *ACM Transactions on Graphics (TOG)* (2011), vol. 30, ACM, p. 149. 3, 5
- [RGM\*12] RODRIGUEZ M. B., GOBBETTI E., MARTON F., PINTUS R., PINTORE G., TINTI A.: Interactive exploration of gigantic point clouds on mobile devices. In *VAST* (2012), pp. 57–64. 2
- [RH10] RYDE J., HU H.: 3d mapping with multi-resolution occupied voxel lists. *Autonomous Robots* 28, 2 (2010), 169. 2
- [RSB93] RIVEST J.-F., SOILLE P., BEUCHER S.: Morphological gradients. *J. Electronic Imaging* 2, 4 (1993), 326–336. 4
- [SB97] SMITH S. M., BRADY J. M.: SusanãA new approach to low level image processing. *International journal of computer vision* 23, 1 (1997), 45–78. 4
- [SNF\*13] SHUMAN D. I., NARANG S. K., FROSSARD P., ORTEGA A., VANDERGHEYNST P.: The emerging field of signal processing on graphs: Extending high-dimensional data analysis to networks and other irregular domains. *IEEE Signal Processing Magazine* 30, 3 (2013), 83–98. 5

- [SZW09] SCHEIBLAUER C., ZIMMERMANN N., WIMMER M.: Interactive domitilla catacomb exploration. In *Proceedings of the 10th International conference on Virtual Reality, Archaeology and Cultural Heritage* (2009), Eurographics Association, pp. 65–72. 2
- [TM98] TOMASI C., MANDUCHI R.: Bilateral filtering for gray and color images. In *Computer Vision, 1998. Sixth International Conference on* (1998), IEEE, pp. 839–846. 4
- [Uli88] ULICHNEY R. A.: Dithering with blue noise. *Proceedings of the IEEE* 76, 1 (1988), 56–79. 3



**Figure 9:** Surfaces reconstructed using [BL17] from the proposed curvature-aware resampling. Top : Statues inside the Eim Ya Kyaung temple and close-up view of the details of the cape. Bottom : Statue inside the Khaymingha temple and close-up view of the quality of the triangulation produced, a direct consequence of the good distribution of samples.